Chain stiffness boosts active nanoparticle transport in polymer networks

Xue-Zheng Cao [1,*], Holger Merlitz,[2] Chen-Xu Wu [1], and M. Gregory Forest[3]

[1]*Department of Physics, Xiamen University, Xiamen 361005, People's Republic of China*
[2]*Leibniz-Institut für Polymerforschung Dresden, 01069 Dresden, Germany*
[3]*Departments of Mathematics, Applied Physical Sciences, Biomedical Engineering, University of North Carolina at Chapel Hill, Chapel Hill, North Carolina 27599-3250, USA*

Recent advances in technologies such as nanomanufacturing and nanorobotics have opened new pathways for the design of active nanoparticles (NPs) capable of penetrating biolayers for biomedical applications, e.g., for drug delivery. The coupling and feedback between active NP motility (with large stochastic increments relative to passive NPs) and the induced nonequilibrium deformation and relaxation responses of the polymer network, spanning scales from the NP to the local structure of the network, remain to be clarified. Using molecular dynamics simulations, combined with a Rouse mode analysis of network chains and position and velocity autocorrelation functions of the NPs, we demonstrate that the mobility of active NPs within cross-linked, concentrated polymer networks is a monotonically increasing function of chain stiffness, contrary to passive NPs, for which chain stiffness suppresses mobility. In flexible networks, active NPs exhibit a behavior similar to passive NPs, with a boost in mobility proportional to the self-propulsion force. These results are suggestive of design strategies for active NP penetration of stiff biopolymer matrices.

I. INTRODUCTION

Biological gels such as mucus that coats various human organs have the remarkable ability to selectively reject versus allow transport of specific molecules, proteins, or pathogens [1–4]. Targeted delivery of inhaled or ingested therapeutic drug-carrier particles must account for the mucus barriers in order to control the uptake by specific cells, tumors, or vasculature [5–7]. One approach is to design the surface chemistry of drug-carrier nanoparticles (NPs) so that they penetrate gel barriers with controlled passage times [8–11]. Chemically neutral NPs in mucus gels transport by passive diffusion with mobility properties dependent on NP size relative to the free volume fraction and pore size distribution of the polymer network. Nanoparticle diffusion is governed by viscous drag for sufficiently small NPs relative to the pore size, steric interactions for NPs commensurate with the mean pore size, and entropic fluctuations of the polymer network for NPs much larger than the pores. In the latter two cases, NP diffusion is strongly influenced if there are attractive or repulsive interactions between the NP surface chemistry and the polymers. For large NPs, the existence of a "shell" of modified polymers surrounding the NP led to the methods of two-bead microrheology, where cross correlations of two nearby beads allow one to extract the equilibrium network properties and filter out the modified signals of individual beads [12]. More inspiration for active NPs in polymers comes from molecular motors fueled by ATP that stochastically walk along microtubules to transport cargo [13,14] and by small proteins that transiently cross-link genes and that extrude loops on chromosomal DNA to densely confine the genome and create gene clusters to perform cellular functions such as homology searches [15,16]. Progress in nanotechnology has also stimulated synthesis of active NPs [17,18] for a broad range of applications at the length scales that biopolymer chains perform biological functions.

Here we consider an alternative scenario in which active nonequilibrium forces between the NP and polymer network drive NP transport, a stochastic variation on active magnetic microbead rheology. In active microbead rheology, an atomic force microscope tip imposes a force direction and amplitude on the microbead [19,20]. Active NPs consume fuel in the system (via either chemical reactions [21–23], light-induced temperature gradients [24,25], or strong repulsive interactions with the polymer network [20]) and convert that energy into locally ballistic increments an order of magnitude larger than increments due to thermal fluctuations of the surrounding polymers. Such strong NP-polymer activity amplifies an otherwise equilibrium NP increment process that underlies passive microrheology (for micron-scale NPs) or nanorheology (for nanometer-scale NPs). This strong NP-polymer activity creates a stochastic analog of active microrheology or nanorheology. With each NP increment, the surrounding polymer network is driven out of equilibrium and the nonlinear response of the network imparts a direction to the force which again is amplified by NP fuel consumption. Were the network a simple viscous fluid, this NP behavior would simply reduce to Brownian motion with an amplified temperature [26]; in that case, all NP transport statistics are known and the medium itself never stores any stress, so all increments are uncorrelated. However, in a polymer network, the nonlinear viscous and elastic response of the network couples with the amplified deformation and stress generated by the NP in

---
*xzcao@xmu.edu.cn

every stochastic increment. Below we model this stochastic analog of active NP rheology to explore the mobilities of NPs with diameters equal to three monomers, comparable to the averaged pore size of the cross-linked concentrated polymer network, for polymer networks that are relatively stiff and gel-like. We show how the stiffness of the polymer network strongly affects the diffusive scaling of active stochastic NPs, which turn increasingly superdiffusive above an active force threshold, reducing the NP passage times through the network [27].

II. MODEL AND METHODS

A. Simulation model of polymer chains and NPs

In the simulations, a polymer chain is composed of Lennard-Jones (LJ) spheres representing Kuhn monomers that are connected by anharmonic springs governed by a finitely extensible nonlinear elastic (FENE) potential [28], defined as

$$U_{\text{FENE}}(r) = -0.5\kappa R_0^2 \ln\left[1 - \left(\frac{r}{R_0}\right)^2\right]$$
$$+ 4\varepsilon_0\left[\left(\frac{\sigma_m}{r}\right)^{12} - \left(\frac{\sigma_m}{r}\right)^6\right] + \varepsilon_0, \quad r < R_0, \quad (1)$$

where $\kappa = 30\varepsilon_0/\sigma_m^2$ is the spring constant, ε_0 is the energy unit, and $R_0 = 1.5\sigma_m$ is the maximum pair length of bonded neighboring monomers to prohibit a break of polymer chains. By adopting the FENE bond potential, the averaged bond length is set to $\langle l_{\text{bond}}\rangle = 0.97\sigma_0$, where σ_0 is the length unit of the modeling system. The monomer diameter is $\sigma_M/\sigma_0 = 1$ and NPs are larger with $\sigma_{NP}/\sigma_0 = 3$. Note that the NP diameter is chosen to be larger than one monomer length and comparable to the mesh size of the studied polymer network as described below. Energies are expressed in units of kT, with the Boltzmann constant $k = 1$, and the temperature is fixed at $T/T_0 = 1$, with T_0 being the temperature unit. Interparticle pair interactions are LJ potentials, truncated at their minima $r_c = 1.12\sigma_{ij}$ to approximate an implicit athermal solvent [29]. The monomer-monomer, NP-monomer, and NP-NP interactions are modeled as truncated and shifted LJ potentials

$$U_{\text{LJ}}(r) = 4\varepsilon_0\left[\left(\frac{\sigma_{ij}}{r}\right)^{12} - \left(\frac{\sigma_{ij}}{r}\right)^6 - \left(\frac{\sigma_{ij}}{r_c}\right)^{12}\right.$$
$$\left. + \left(\frac{\sigma_{ij}}{r_c}\right)^6\right], \quad r < r_c, \quad (2)$$

where $\sigma_{ij} = \sigma_0$, $\sigma_{ij} = \sigma_M + \sigma_{NP}$, and $\sigma_{ij} = \sigma_{NP}$ stand for the mean size of two particles (ith and jth) involved in the monomer-monomer, NP-NP, and NP-monomer pair interactions, respectively. The parameter $r_c = 2^{1/6}\sigma_{ij}$ is the cutoff distance. It is easily verified that with this cutoff implemented, the attractive contribution to this potential is eliminated, i.e., $U_{\text{LJ}}(r) = 0$ when $r > r_c$. The stiffness of polymer chains is governed by defining the bending potential between every two neighboring bonds

$$U_{\text{b}}(\theta) = \varepsilon_{\text{b}}(\theta - \pi)^2, \quad (3)$$

where θ is the angle between the two bonds. A larger bending potential coefficient ε_{b} corresponds to stiffer polymers. Via computing the bond-bond correlation function, it is confirmed

in our simulations that the persistence length l_p is linearly proportional to ε_{b}, when $\varepsilon_{\text{b}}/kT > 2$, for the adopted chain model. In addition, $l_p = 2\sigma_0$, $4\sigma_0$, and $8\sigma_0$ when $\varepsilon_{\text{b}}/kT = 2$, 4, and 8, respectively.

The equation of motion for the displacement of a passive monomer with index i is given by the Langevin equation [30,31]

$$m_i \frac{d^2\mathbf{r}_i}{dt^2} = -\nabla U_i - \zeta \frac{d\mathbf{r}_i}{dt} + \mathbf{F}_i, \quad (4)$$

where $m_i = m_0$ for monomers, $\mathbf{r}_i$ is the position of the ith monomer, and U_i is the total conservative potential energy acting on the ith monomer. The quantity $\mathbf{F}_i$ is a random external force without drift and a second moment proportional to the temperature and the friction constant ζ. For the active NP, there is an additional force pointing into the current direction of its velocity vector,

$$m_{NP} \frac{d^2\mathbf{r}_{NP}}{dt^2} = -\nabla U_{NP} - \zeta \frac{d\mathbf{r}_{NP}}{dt} + \mathbf{F}_{NP} + f_{\text{sp}}\mathbf{e}_v(t), \quad (5)$$

where $\mathbf{e}_v(t)$ is the unit vector of the active NP's instantaneous velocity at time t, and f_{sp} gives the value of self-propelling force. In our simulations, the temperature is fixed at $T = 1$, a time step $\Delta t = 0.005\tau_0$, and the friction coefficient $\zeta = \tau_0^{-1}$ is implemented. Note that hydrodynamic interactions are not considered in the present study. The masses of the particles are set to $m_M/m_0 = 1$ (monomers) and $m_{NP}/m_0 = 27$ (nanoparticle), with m_0 the mass unit. The temperature is then normalized to that energy unit using a Boltzmann constant $k_B = 1$ with the temperature unit $T_0 = \varepsilon_0/k_B$. The time unit is given by $\tau_0 = \sigma_0(m_0/\varepsilon_0)^{1/2}$. The force unit is given by $f_0 = \varepsilon_0/\sigma_0$ and all forces given in the paper are multiples of this unit.

B. Network creation and NP activation

All simulations start from a phase in which polymer chains are distributed homogeneously in a cubic box with periodic boundary conditions in all directions and the initial bulk number density of monomers is $n_m = N_m/V = 0.051$, where V and N_m are the system volume and the total number of monomers included in the system, respectively. The molecular weights of polymer chains are fixed at $N = 512$, with the corresponding critical number density of monomers crossing over from the dilute to the semidilute regime being at $n_m^* = \frac{3}{4\pi N^{0.5}} \approx 0.010$. Individual polymer chain coils are interpenetrated into each other in the semidilute regime. To form a regular network, each chain contains 32 cross-linking monomers regularly distributed along the chain, i.e., one cross-linking monomer per subchain of contour length $l_{\text{sub}}^{\text{cr}} = \frac{512}{32} = 16$. These cross-linking monomers serve as binding sites to create permanent intrachain or interchain cross-links (CLs). This approach leads to networks with pore sizes that are sufficiently large to grant passage of the NPs. A NP is initially planted and frozen at the center of the simulation box. A dynamical monitoring of CLs is performed continuously and automatically as the simulation time evolves, with every potential binding site in polymer chains being capable of participating in just one CL. The number of CLs N_{CL} converges to a plateau value when the cross-linking process is completed,
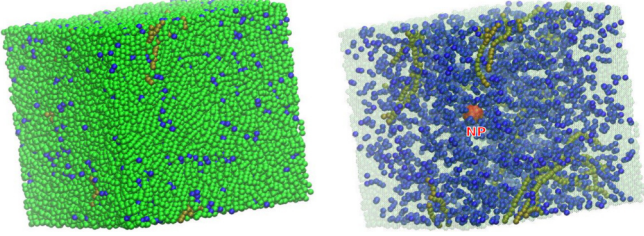
FIG. 1. Modeled system of NPs in a polymer network, with a large red particle, dark blue particles, and light green particles representing the NP, permanent CLs, and non-cross-linked monomers, respectively. In addition, a single polymer chain is colored in dark olive in order to display the configuration taken by individual polymer chains. All components are shown in the left panel, while the non-cross-linked monomers are transparent in the right panel. Here the bending energy between neighboring bonds, governing the stiffness of polymer chains, is at $\varepsilon_b/kT = 8$ and the bulk number densities of monomers and permanent CLs are given by $n_m = 0.80$ and $n_{CL} = 0.026$, respectively.

i.e., close to all binding sites have reacted. We then halt the cross-linking kinetics and compress the simulation box size to obtain a concentrated polymer phase with homogeneous densities of monomers and CLs as shown in Fig. 1.

In simulations, each system is relaxed by a simulation run of the order of $10^3 \tau_{sub}$, where $\tau_{sub} \sim l_{sub}^{cr2}$ is the configurational relaxation time of polymer subchains with contour length l_{sub}^{cr}, i.e., the length of polymer strands between neighboring cross-links. The τ_{sub} value, defining the time for the system to reach equilibrium, is determined from calculating the stress relaxation modulus $G(t)$ of an un-cross-linked polymer melt at the same concentration $n_m = 0.80$. Subsequently, a much longer run (of the order of $10^6 \tau_{sub}$) of data acquisition is performed, during which a trajectory of thousands of conformations is stored for the data analysis of the statistical properties of the active NP and the viscoelastic behavior induced by the active NP on the polymer networks. Starting from the equilibrium condition obtained above, we activate the NP and introduce a self-propelling force acting along its velocity (or last increment) vector, as defined by Eq. (5). In a set of simulations we study the variations in NP mobility due to polymer chain stiffness and as a function of the amplitude of the NP's self-propelling force.

III. RESULTS AND DISCUSSION

A. Enhanced motion of active NPs

It is well known that the motion of a NP, immersed in a polymer melt or a concentrated polymer network, is coupled to the dynamic structural relaxation of surrounding polymer subchains [32–34]. A necessary condition for the NP to pass through the permanent network is that the subchain contour length between neighboring cross-links, l_{sub}^{cr}, exceeds the diameter of the NP, σ_{NP}. The critical timescale τ_{re}^{cr} for a passive NP to escape from being trapped by polymer chains is of the same order of magnitude as the relaxation time τ_{sub} of subchains with end-to-end distance equal to the NP diameter. In addition to the permanent cross-links, individual polymer strands among cross-links may impose topological obstacles

on each other, e.g. entanglements [35]. The presence of entanglements delays the structural relaxation of polymer chains on length scales above the entanglement length l_{ent}, which is defined as the averaged contour length of polymer subchains between neighboring entanglements. Note that the number of entanglements increases and thus the corresponding entanglement length l_{ent} decreases with increasing persistence length (stiffness) of polymer chains [36], which possibly results in the smaller size of entanglement length compared to the NP diameter, as confirmed below by performing Rouse mode analysis to detect the relaxation spectrum of polymer networks at $\varepsilon_b/kT = 4$ and 8. Therefore, increasing the stiffness of polymer chains has a scenario of effectively immobilizing the passive NP due to chain entanglements when $l_{ent} < \sigma_{NP} < l_{sub}^{cr}$, though the separations between permanent cross-links are large enough for the NP to escape. Figure 2(a) shows such an example in which the trajectories of a passive NP inside a stiff polymer network remain confined within a small volume of the same order as the NP size. In such a situation, an active force is required for the NP to escape confinement. Furthermore, the corresponding self-propelling force f_{sp} of the active NP has to exceed the trapping force f_{trap} induced by the surrounding polymer segments in order to overcome the stiff network barrier constraint.

When a self-propelling force acts on the NP, as shown in Fig. 2(b), the position increments exhibit stochastic fluctuations, superimposed on a persistent ballistic motion over distances larger than the NP diameter. This allows the NP to overcome the trapping barrier induced by the stiff polymer chains on the same timescales. On longer timescales, the position increments of the self-propelling NP reveal a zigzag pattern, reflecting the elastic feedback induced by every increment as the stiff polymer network is driven out of equilibrium by the active NP, after which the stored elastic stress pushes back in the direction opposite to the last increment. Thus one observes a correlation in the increments, similar to the mechanisms behind passive microbead rheology in polymer networks and solutions, but now with larger increments due to both the strong NP propulsion force and the stiff elastic response of the network. Note further that the amplitudes of the NP increments diminish as the network stiffness is weakened, as visible when comparing Figs. 2(b) and 2(c). The self-propelling NP covers longer distances in the stiff polymer network over the same time interval.

To quantify the NP mobility, the averaged mean square displacement (MSD) of a self-propelled NP in a stiff polymer network with varying self-propelling forces,

$$g(t) = \langle [r(t + t_0) - r(t_0)]^2 \rangle, \tag{6}$$

is computed and presented in Fig. 3(a). With constant stiffness of polymer chains and varying propulsion force f_{sp}, the NP ballistic regime [defined by the short-term superdiffusive scaling $g(t) \sim t^\gamma$ with $\gamma \approx 2$] persists over longer lag times before crossing over into the subdiffusive regime [$g(t) \sim t^\gamma$ with $\gamma < 1$]. The MSD $g(t)$ versus f_{sp} plot confirms that the self-propelling force has to exceed a critical value, the trapping force, in order to "unlock" a trapped NP on those timescales in a stiff polymer network: There is almost no propagation ($\gamma \approx 0$) in the subdiffusive regime, at which ($\gamma \approx 0$) and $g(t) \approx \sigma_0^2$ for lag times of $t < t_{rel}^{NP}$, when $f_{sp}/f_0 \leqslant 40$. Note
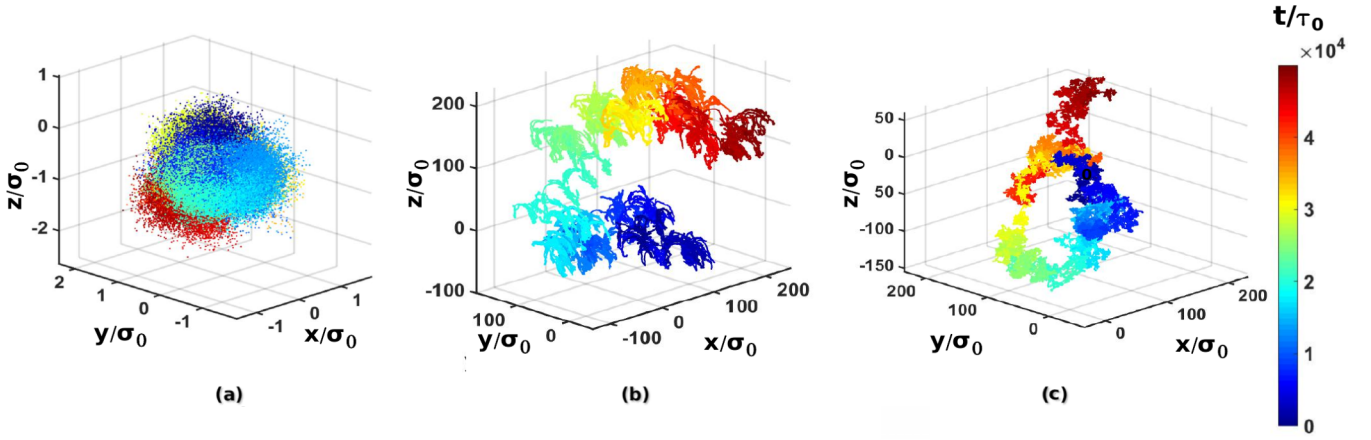
FIG. 2. Examples of NP trajectories within identical time intervals. (a) Passive NP inside a stiff polymer network with a constant bending energy between neighboring bonds of $\varepsilon_b/kT = 8$. (b) Self-propelled NP inside a stiff polymer network with $f_{sp}/f_0 = 100$ and $\varepsilon_b/kT = 8$. Note the different scales of the axes and the considerably longer position increments of the NP. (c) Self-propelled NP inside a flexible polymer network with driving force $f_{sp}/f_0 = 100$ and bending energy constant $\varepsilon_b/kT = 1$. The monomer density $n_m = 0.80$ and the CL density $n_{CL} = 0.026$.

that $t_{rel}^{NP} \approx 10^4 \tau_0$ is related to the structural relaxation time of polymer subchains of size comparable to the NP diameter. With large driving forces $f_{sp}/f_0 \geqslant 50$, the crossover of the NP motion from subdiffusion with $\gamma < 1$ to linear diffusion with $\gamma = 1$ occurs at a lag time shorter than t_{rel}^{NP}, indicating that the NP has already pushed through the barrier before the structural relaxation of the polymer subchains has occurred. Therefore, there exists a threshold of the self-propelling force, specifically between $f_{sp}/f_0 = 40$ and 50 at chain stiffness $\varepsilon_b/kT = 8$, above which the NP motion decouples from the dynamical structural relaxation of polymer subchains. Furthermore, due to the stochasticity of the active increment process, the ballistic motion is of finite duration: Even at the highest driving force $f_{sp}/f_0 = 100$, as shown in Fig. 3, the NP leaves its ballistic propagation regime and crosses

over to a subdiffusive regime. The timescale at which the constraining effect of the stiff network disturbs the ballistic NP motion can be shortened, by softening the network chains, as shown in Fig. 4(a). Hence, the duration of the ballistic motion (persistence time) of the NP is an increasing function of network stiffness. This effect is opposite to the results for passive NPs where mobility is a monotonically decreasing function of network stiffness [see Fig. 4(b)]. Thus there is a
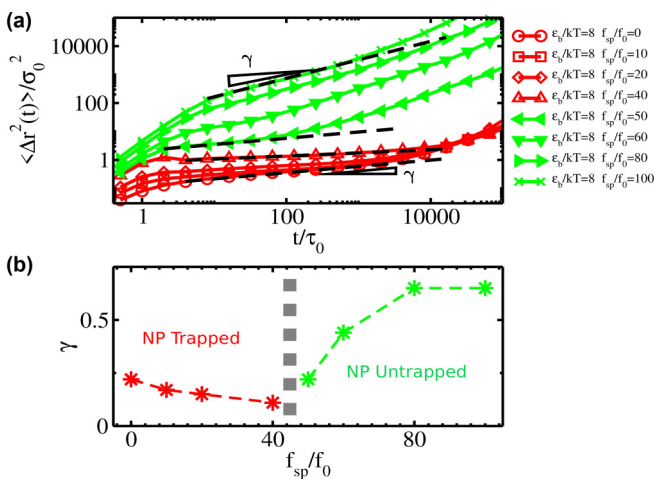

FIG. 3. (a) Averaged mean square displacements of a NP diffusing in a stiff polymer network with $\varepsilon_b/kT = 8$, at varying self-propelling forces of the NP. (b) Power exponent, indicating subdiffusion as shown by the black straight dashed lines in the intermediate time regime of (a), plotted against the self-propelling force. Here $n_m = 0.80$ and $n_{CL} = 0.026$.
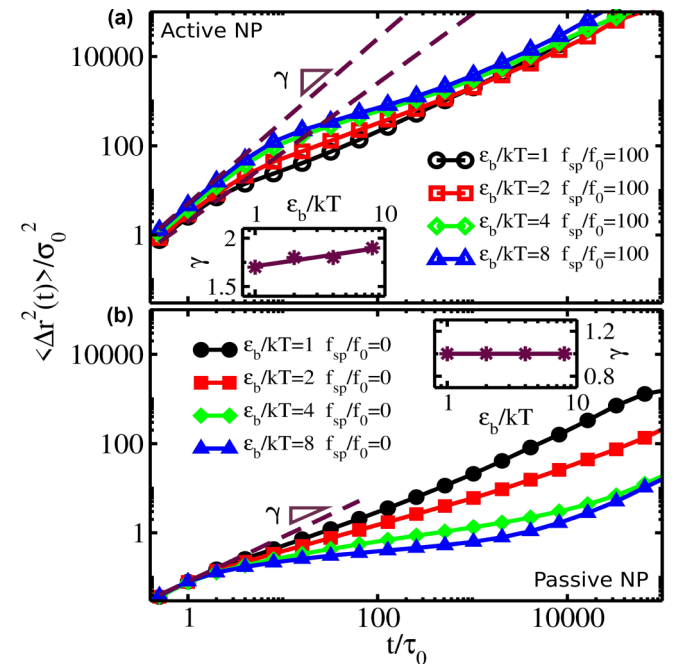

FIG. 4. Mean square displacements of (a) an active NP with $f_{NP}/f_0 = 100$ and (b) a passive NP with $f_{NP}/f_0 = 0$, diffusing in networks of various degrees of stiffness. The insets display the power exponents as shown by the maroon straight dashed lines in the short-time regime, which is diffusive ($\gamma = 1$) for passive particles and nearly ballistic ($\gamma \approx 2$) for driven particles. The monomer density $n_m = 0.80$ and the CL density $n_{CL} = 0.026$.
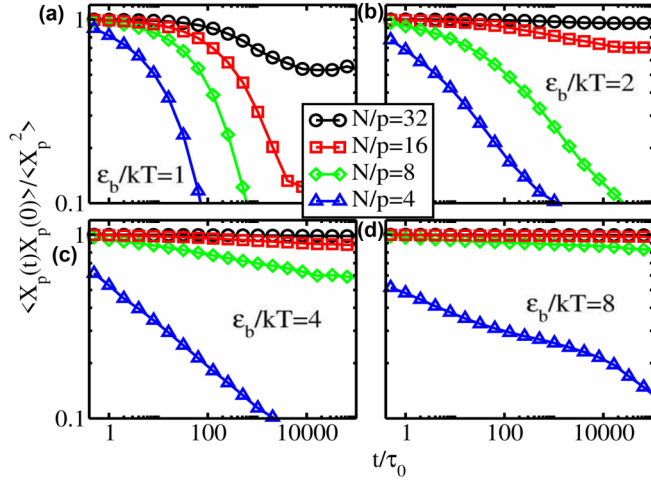
FIG. 5. Averaged autocorrelation functions of the Rouse modes of network chains on different length scales and at various degrees of chain stiffness. Here $N = 512$ is the length of individual polymer chains, and the minimum mesh size of polymer network, i.e., the polymer subchain contour length between two neighboring cross-links, is at $l_{sub}^{cr} = \frac{N}{P} = 16$, $n_m = 0.80$, and $n_{CL} = 0.026$.

clear cooperative effect, a positive feedback, between stiffness of the network and the NP self-propelling force.

B. Interaction of active NPs with polymer networks

To correlate the structural relaxation spectrum of polymer chains to the trapping effect of polymer subchains on the NP, we perform a Rouse mode analysis for the relaxation dynamics of polymer chains in the network [37]. The pth Rouse mode is computed as

$$X_p(t) = \left(\frac{2}{N}\right)^{1/2} \sum_{i=1}^{N} r_i \cos\left[\frac{p\pi}{N}\left(i - \frac{1}{2}\right)\right]. \quad (7)$$

The averaged autocorrelation functions $\langle X_p(t) \cdot X_p(0)\rangle / \langle X_p^2\rangle$ are presented in Fig. 5. In the Rouse mode analysis, the pth mode corresponds to the structural relaxation of a sub-chain containing $(N - 1)/p$ monomers, while the $p = 0$ mode corresponds to the center of mass of the entire chain. In the case of a polymer network consisting of flexible chains, i.e., $\varepsilon_b/kT = 1$ [Fig. 5(a)], the conformations of subunits of contour lengths shorter than the cross-linking length $l_{cr} = 16$ are relaxing. On length scales beyond l_{cr}, however, such a relaxation is hindered by the presence of the (permanent) cross-links of the polymer network. These networks are unable to trap a NP, as long as its size remains smaller than the mesh size l_{cr}, since the structural relaxation of polymer sub-chains occasionally opens a gate to release the NP. Increasing the chain stiffness, we find the minimum unrelaxed structure of polymer subchains shifts to shorter length scales due to the presence of entanglements of polymer strands among cross-links. In the case of $\varepsilon_b/kT = 8$, the polymer subchains relax only on length scales comparable to or smaller than the NP size, while their structure is physically frozen on relatively larger length scales; the polymer chains thereby have the ability to arrest the motion of a passive NP.
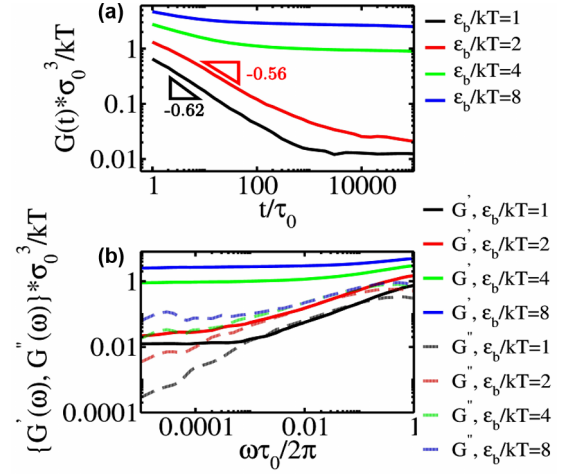

FIG. 6. Viscoelastic property of polymer networks at various degrees of chain stiffness: (a) stress relaxation moduli of the poly-mer network and (b) corresponding storage and loss moduli. Here $n_m = 0.80$ and $n_{CL} = 0.026$.

The trapping effect that constrains a NP inside a stiff poly-mer network is a result of the NP's inability to elastically deform the surrounding polymer chains that form its cage for a sufficiently long time that its entropic fluctuations find an opening. In order to investigate the mechanism that is responsible for the trapping effect of polymer subchains on the NP, we compute both the elastic and viscous moduli of the network. In the simulations, the pressure tensor is computed as a six-element vector. The six components of the vector are ordered σ_{xx}, σ_{yy}, σ_{zz}, σ_{xy}, σ_{xz}, and σ_{yz}. The equation for the I and J components (where I and $J = x, y, z$) is given by a combination of the kinetic energy tensor and the virial tensor

$$\sigma_{IJ} = \frac{\sum_k^{NB} m_k v_{kI} v_{kJ}}{V} + \frac{\sum_k^{NB} r_{kI} f_{kJ}}{V}, \quad (8)$$

where NB gives the number of all particles including NPs and monomers contained in the system and V is the system vol-ume. Here r_{KI} and f_{kI} are the Ith elements of the position and force vector of the kth particle, respectively. The virial term, which includes energy contributions except for the kinetic energy as given by the first term, is the sum of contributions of pair and bond interactions to the force on individual beads. The computed tensors for the stress relaxation modulus are stored after the system converges to equilibrium. We first com-pute the stress relaxation modulus $G(t)$. There is a standard protocol of relating $G(t)$ to the stress autocorrelation function $\mathcal{S}(t)$ of the off-diagonal elements of the system's stress tensor, based on the Green-Kubo relation [36,38,39]

$$G(t) = \frac{V}{3k_BT}[\langle\sigma_{xy}(t)\sigma_{xy}(0)\rangle + \langle\sigma_{yz}(t)\sigma_{yz}(0)\rangle$$
$$+ \langle\sigma_{xz}(t)\sigma_{xz}(0)\rangle], \quad (9)$$

with σ_{xy}, σ_{yz}, and σ_{xz} the off-diagonal elements of the system tensor. As revealed in Fig. 6, the plateau modulus at large lag times in $G(t)$ for relatively flexible polymer chains, with $\varepsilon_b/kT = 1$ and 2, arises due to the unrelaxed cross-linking structure of the permanent network. By contrast, the unrelaxed structure of the network due to dense entanglements of stiff

polymer chains, with $\varepsilon_b/kT = 4$ and 8, results in plateaus at smaller timescales. We then compute the complex modulus $G^*(\omega)$, the Fourier transform of the stress relaxation function $G(t)$, with the storage (elastic) modulus $G'(\omega)$ and loss (viscous) modulus $G''(\omega)$ given by the real and imaginary parts

$$G^*(\omega) = G'(\omega) + iG''(\omega), \tag{10}$$

where $\omega = 2\pi/t$ is the angular frequency. The results of

$$G'(\omega) = G_p + \omega \int_0^\infty [G(t) - G_p] \sin(\omega t)dt,$$

$$G''(\omega) = \omega \int_0^\infty [G(t) - G_p] \cos(\omega t)dt, \tag{11}$$

where G_p is the plateau modulus, are shown in Fig. 6(b). The figures reveal the polymer network of flexible chains: at high frequencies, Rouse-like characteristics of a transition state between sol and gel phases, with $G' \approx G''$, and at low frequencies, elasticity-dominated gel characteristics, with $G' \gg G''$. However, the polymer network is elasticity dominated and gel-like in the full range of frequencies for sufficiently stiff polymer chains, $\varepsilon_b/kT = 4$ or 8.

The strong elastic gel characteristics of stiffer networks imply that the self-propelling NP forcing is primarily resisted by the elastic restoring force of the deformed polymer strands, more so than the viscous drag force of the network. Furthermore, in the "wake" of the NP increment, there is a propensity for the stiff chains to tend to align with the direction of previous increments, while permanent cross-links are compressed along the leading edge of the NP increment and build up an elastic restoring force [40]. This nonequilibrium deformation induces a bias for the NP to recoil, once the stored elastic network stress exceeds the NP self-propulsion force, preferentially along the path of those previous increments. Over whatever timescale it takes for this anisotropic deformation and stress to accumulate and exceed the NP propulsion force, the NP recoils, biased by the anisotropy in the network alignment and stress. To visualize the mobility patterns of a passive or active NP in stiff versus flexible polymer networks, we plot the NP increment time series along each of the x, y, and z axes, as shown in Fig. 7(a). There is essentially zero mobility of a passive NP in a sufficiently stiff polymer network, whereas an active NP is visibly mobile for a high self-propelling force $f_{sp}/f_0 = 100$. Furthermore, the active NP reverses direction on timescales of several increments, reflecting the buildup of an elastic restoring force from the nonequilibrium deformation of the stiff network that exceeds the NP's self-propelling force, persisting until the stored stress relaxes. As sketched in Figs. 7(b) and 7(c), the elastic rebound phenomenon observed in a stiff polymer network with $G' \gg G''$ is absent for the same self-propelled NP in a flexible polymer network, where the elastic and viscous moduli are comparable, $G' \approx G''$.

C. Tubelike channel

Contrary to the motion of a passive particle that is driven by thermal fluctuations, active NPs with a sufficiently large self-propelling force $f_{sp} > f_{trap}$ deform the surrounding polymer subchains to align in its wake with the direction of its previous increment, which is the direction of the self-propelling force.
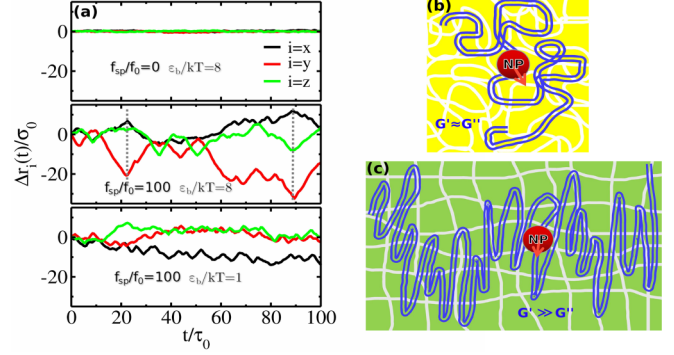

FIG. 7. Mobility patterns of active and passive NPs. (a) One-dimensional trajectories of passive ($f_{sp}/f_0 = 0$) and active ($f_{sp}/f_0 = 100$) NP positions in flexible ($\varepsilon_b/kT = 1$) and stiff ($\varepsilon_b/kT = 8$) polymer networks. The dashed gray lines in the middle panel are plotted to show U-turn moments of active NPs diffusing in a stiff polymer network. Here $n_m = 0.80$ and $n_{CL} = 0.026$. (b) Sketch of an active NP randomly diffusing in a viscoelastic network consisting of flexible polymer chains. (c) Sketch of an active NP diffusing and rebounding in an elastic gel-like network consisting of stiff polymer chains.

This actions of the network and the NP occur on a timescale shorter than the structural relaxation time of the subchains and thus the NP motion is uncoupled from the structural relaxation. During this time, the network's elastic and viscous moduli resist the NP, while the self-propelled NP is driving the network out of equilibrium as it deforms chains. In this process, stiffer networks store more deformational stress and are more prone to induce chain alignment along the path of the NP, while energy is lost due to the viscous drag on the NP. In flexible polymer networks, polymer strands surrounding the NP are easily displaced by the advancing NP and the viscous drag force is the dominant resistance to the NP motion. As a result, the NP trajectory resembles a three-dimensional diffusion due to random collisions with surrounding monomers. However, inside a stiff polymer network, fluctuations perpendicular to the increments of the NP are suppressed by the bending resistance of the polymer strands. Thus, once a threshold driving force is passed, the NP-network interaction establishes an effective local tubelike channel for the NP motion with its instantaneous moving direction along the path of the previous few increments. The self-propelling NP's motion in the tubelike channel is similar to the directional motion of self-propelled stiff filaments that are confined to move along the path of their contour lengths in crowded environments [41].

To explore the existence of a tubelike channel for the superdiffusive motion of a self-propelling NP in stiff polymer networks, the time-dependent averaged autocorrelation functions of the NP's velocity and position vectors are computed as

$$g_{vel}(t) = \langle |e_x(t)e_x(0) + e_y(t)e_y(0) + e_z(t)e_z(0)| \rangle,$$

$$g_{cor}(t) = \langle |u_x(t)u_x(0) + u_y(t)u_y(0) + u_z(t)u_z(0)| \rangle, \tag{12}$$

with (e_x, e_y, e_z) and (u_x, u_y, u_z) the unit vectors of the NP velocity and position increment, respectively. Note that our aim here is to detect the dimensionality of the NP's motion,
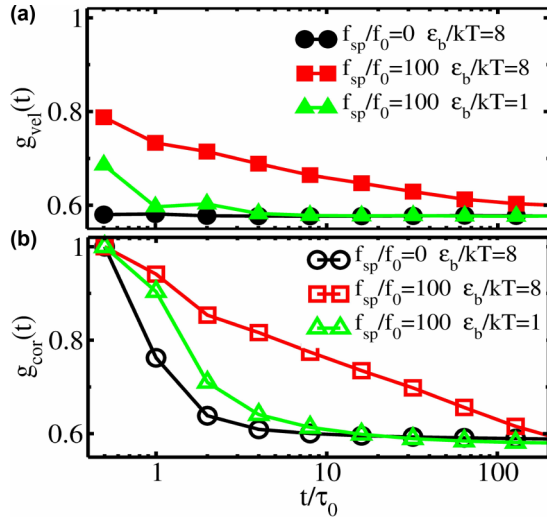
FIG. 8. Averaged autocorrelation functions of the unit vectors of (a) velocity and (b) position of an active (inactive) NP diffusing in a flexible (stiff) polymer network. Here $n_m = 0.80$ and $n_{CL} = 0.026$.

without distinguishing between opposite directions of the vectors in the correlation computations. That is why absolute values are used in the above correlation functions. With the absolute value being considered, the dot product of two unit vectors remains invariant if we replace the angle between the two vectors, θ, by $\pi - \theta$. Theoretically, the autocorrelation function should converge to 0.5 at very large timescales when the memory is lost completely. The corresponding results are shown in Fig. 8: The autocorrelation functions of driven NPs inside stiff networks decay significantly slower when compared to driven NPs in flexible networks or to passive NPs. This implies that the superdiffusive motion of the NP persists longer in sufficiently stiff networks, supporting the tubelike network deformation induced by sufficiently strong self-propelling force of the NP. Note that the trajectory of a self-propelling NP in a stiff polymer network after every rebouncing does not match completely its moving route prior to the turning point, since the elastic stretching interaction between the NP and polymer chains does not perfectly align with the NP velocity due to the NP's viscous interaction with polymer network; therefore, the NP's one-dimensional to and fro movement resembles a zigzag. In flexible networks, the nonequilibrium deformations induced by active NP increments quickly decorrelate as those network length scales relax rapidly.

IV. CONCLUSION

In summary, our investigation shows that the transport efficiency of an active particle inside a dense polymer network increases with the chain stiffness. This counterintuitive behavior is ascribed to a one-dimensional ballistic motion through a tubelike channel, confined by the surrounding polymer strands that remain unrelaxed on the timescale the active particle pushes through. Contrary to that, inside a flexible network, the same active particle undergoes a three-dimensional Brownian motion that reduces its propagation efficiency. At a given self-propelling force, the persistence length of the NP's ballistic motion increases with the chain stiffness of the polymer network. Our Rouse mode analysis and the stress relaxation moduli confirm that a stiffening of the polymer chains makes the polymer network rather gel-like with stronger contribution of elasticity. For a NP in such a network, the tension it exerts onto the confining polymer strands induces an elasticity-dominated resistance which may eventually reverse the direction of the particle's motion, while at the same time any propagation into directions perpendicular to the self-propelling force is hindered by the resistance from unrelaxed polymer subchains on length scales comparable to or shorter than the NP size, resulting in the NP's one-dimensional to and fro motion pattern. Inside a flexible polymer network, however, the particle collides randomly with monomers, and in the absence of elastic contributions, the effective forces acting on the particle are viscous and dissipative, causing the NP to exhibit an effective three-dimensional isotropic Brownian motion. The investigation of autocorrelation functions of the active walker's position and velocity vectors confirms the increased persistence of ballistic motion inside stiff networks. While the fast decay of these correlation functions of a self-propelled particle resembles that of a passive Brownian walker in flexible networks, these correlation functions display a slower decay when the active particle propagates in stiff networks. Our study has shed light on the correlation between the viscous and elastic properties of polymer networks and the propagation of self-propelled particles therein, providing theoretical and computational insights into a goal-driven design of synthetic nanomotors in crowded environments. Given that the rigidity of polymer chains can be modified by simply tuning temperature and/or water content, this study offers directives for a cellular level drug delivery in biological systems [42–47].

[1] B. C. Tang, M. Dawson, S. K. Lai, Y.-Y. Wang, J. S. Suk, M. Yang, P. Zeitlin, M. P. Boyle, J. Fu, and J. Hanes, Proc. Natl. Acad. Sci. U.S.A. **106**, 19268 (2009).

[2] O. Lieleg and K. Ribbeck, Trends Cell Biol. **21**, 543 (2011).

[3] C. S. Schneider, Q. Xu, N. J. Boylan, J. Chisholm, B. C. Tang, B. S. Schuster, A. Henning, L. M. Ensign, E. Lee, P. Adstamongkonkul *et al.*, Sci. Adv. **3**, e1601556 (2017).

[4] R. Bansil and B. S. Turner, Adv. Drug Delivery Rev. **124**, 3 (2018).

[5] L. M. Ensign, C. Schneider, J. S. Suk, R. Cone, and J. Hanes, Adv. Mater. **24**, 3887 (2012).

[6] J. M. Newby, I. Seim, M. Lysy, Y. Ling, J. Huckaby, S. K. Lai, and M. G. Forest, Adv. Drug Delivery Rev. **124**, 64 (2018).

[7] E. Fernández Fernández, B. Santos-Carballal, C. De Santi, J. M. Ramsey, R. MacLoughlin, S.-A. Cryan, and C. M. Greene, Materials **11**, 122 (2018).

[8] C. P. Goodrich, M. P. Brenner, and K. Ribbeck, Nat. Commun. **9**, 4348 (2018).

[9] I. Santiago, Nano Today **19**, 11 (2018).

[10] F. Xu, J. M. Newby, J. L. Schiller, H. A. Schroeder, T. Wessler, A. Chen, M. G. Forest, and S. K. Lai, ACS Infect. Dis. **5**, 1570 (2019).

[11] J. Leal, X. Peng, X. Liu, D. Arasappan, D. C. Wylie, S. H. Schwartz, J. J. Fullmer, B. C. McWilliams, H. D. Smyth, and D. Ghosh, J. Control. Release **332**, 457 (2020).

[12] J. M. Newby, A. M. Schaefer, P. T. Lee, M. G. Forest, and S. K. Lai, Proc. Natl. Acad. Sci. U.S.A. **115**, 9026 (2018).

[13] J. R. Baylis, J. H. Yeon, M. H. Thomson, A. Kazerooni, X. Wang, A. E. S. John, E. B. Lim, D. Chien, A. Lee, J. Q. Zhang *et al.*, Sci. Adv. **1**, e1500379 (2015).

[14] A. Somasundar, S. Ghosh, F. Mohajerani, L. N. Massenburg, T. Yang, P. S. Cremer, D. Velegol, and A. Sen, Nat. Nanotechnol. **14**, 1129 (2019).

[15] C. Hult, D. Adalsteinsson, P. A. Vasquez, J. Lawrimore, M. Bennett, A. York, D. Cook, E. Yeh, M. G. Forest, and K. Bloom, Nucleic Acids Res. **45**, 11159 (2017).

[16] Y. He, J. Lawrimore, D. Cook, E. E. Van Gorder, S. C. De Larimat, D. Adalsteinsson, M. G. Forest, and K. Bloom, Nucleic Acids Res. **48**, 11284 (2020).

[17] D. Yamamoto and A. Shioi, KONA Powder Part. J. **32**, 2 (2015).

[18] C. Bechinger, R. Di Leonardo, H. Löwen, C. Reichhardt, G. Volpe, and G. Volpe, Rev. Mod. Phys. **88**, 045006 (2016).

[19] A. A. Solovev, W. Xi, D. H. Gracias, S. M. Harazim, C. Deneke, S. Sanchez, and O. G. Schmidt, ACS Nano **6**, 1751 (2012).

[20] M. Guix, S. M. Weiz, O. G. Schmidt, and M. Medina-Sánchez, Part. Part. Syst. Char. **35**, 1700382 (2018).

[21] J. R. Howse, R. A. L. Jones, A. J. Ryan, T. Gough, R. Vafabakhsh, and R. Golestanian, Phys. Rev. Lett. **99**, 048102 (2007).

[22] W. Gao, A. Pei, R. Dong, and J. Wang, J. Am. Chem. Soc. **136**, 2276 (2014).

[23] J. Katuri, X. Ma, M. M. Stanton, and S. Sánchez, Acc. Chem. Res. **50**, 2 (2017).

[24] J. Palacci, S. Sacanna, S.-H. Kim, G.-R. Yi, D. Pine, and P. Chaikin, Philos. Trans. R. Soc. A **372**, 20130372 (2014).

[25] C. Lozano, B. Ten Hagen, H. Löwen, and C. Bechinger, Nat. Commun. **7**, 12828 (2016).

[26] M. E. Cates, Rep. Prog. Phys. **75**, 042601 (2012).

[27] C. R. Esther, M. S. Muhlebach, C. Ehre, D. B. Hill, M. C. Wolfgang, M. Kesimer, K. A. Ramsey, M. R. Markovetz, I. C. Garbarine, M. G. Forest *et al.*, Sci. Transl. Med. **11**, eaav3488 (2019).

[28] K. Kremer and G. S. Grest, J. Chem. Phys. **92**, 5057 (1990).

[29] J. D. Weeks, D. Chandler, and H. C. Andersen, J. Chem. Phys. **54**, 5237 (1971).

[30] S. Plimpton, J. Comput. Phys. **117**, 1 (1995).

[31] B. Dünweg and W. Paul, Int. J. Mod. Phys. C **2**, 817 (1991).

[32] C. A. Grabowski and A. Mukhopadhyay, Macromolecules **47**, 7238 (2014).

[33] J. T. Kalathi, U. Yamamoto, K. S. Schweizer, G. S. Grest, and S. K. Kumar, Phys. Rev. Lett. **112**, 108301 (2014).

[34] X.-Z. Cao, H. Merlitz, and C.-X. Wu, J. Phys. Chem. Lett. **8**, 2629 (2017).

[35] M. Rubinstein and R. H. Colby, Polymer Physics (Oxford University Press, Oxford, 2003).

[36] W. B. Lee and K. Kremer, Macromolecules **42**, 6270 (2009).

[37] A. Kopf, B. Dünweg, and W. Paul, J. Chem. Phys. **107**, 6945 (1997).

[38] A. E. Likhtman, S. K. Sukumaran, and J. Ramirez, Macromolecules **40**, 6748 (2007).

[39] N. Iwaoka, K. Hagita, and H. Takano, J. Phys. Soc. Jpn. **84**, 044801 (2015).

[40] P. Chen, Z. Xu, G. Zhu, X. Dai, and L.-T. Yan, Phys. Rev. Lett. **124**, 198102 (2020).

[41] S. Mandal, C. Kurzthaler, T. Franosch, and H. Löwen, Phys. Rev. Lett. **125**, 138002 (2020).

[42] T. M. Allen and P. R. Cullis, Science **303**, 1818 (2004).

[43] C. H. Lee, H. Kim, D. V. Harburg, G. Park, Y. Ma, T. Pan, J. S. Kim, N. Y. Lee, B. H. Kim, K.-I. Jang *et al.*, NPG Asia Mater. **7**, e227 (2015).

[44] J. K. Patra, G. Das, L. F. Fraceto, E. V. R. Campos, M. del Pilar Rodriguez-Torres, L. S. Acosta-Torres, L. A. Diaz-Torres, R. Grillo, M. K. Swamy, S. Sharma *et al.*, J. Nanobiotechnol. **16**, 71 (2018).

[45] J. Y. Oh, H. S. Kim, L. Palanikumar, E. M. Go, B. Jana, S. A. Park, H. Y. Kim, K. Kim, J. K. Seo, S. K. Kwak, C. Kim, S. Kang, and J.-H. Ryu, Nat. Commun. **9**, 4548 (2018).

[46] M. Y. Saleh, N. Prajapati, M. A. DeCoster, and Y. Lvov, Front. Bioeng. Biotechnol. **8**, 451 (2020).

[47] W. Tai, P. Zhao, and X. Gao, Sci. Adv. **6**, eabb0310 (2020).